ENVIRONMENTAL RESEARCH
LETTERS

PURPOSE-LED PUBLISHING™
Celebrating the 20th anniversary of Environmental Research Letters

LETTER • **OPEN ACCESS**

Asymmetric urban–rural continuums (URCs) of Southeast Asian cities

To cite this article: Jin Wang *et al* 2026 *Environ. Res. Lett.* **21** 124040

View the article online for updates and enhancements.

You may also like

- An Analytical Model for Predicting the Rate Performance of Battery Cells Under Mixed Kinetic Control
Hongxuan Wang, Fan Wang and Ming Tang
- Thermal changes along the urban-rural continuums in Southeast Asia
Yuanhui Zhu, Soe W Myint, Jiquan Chen et al.
- The Aragats data acquisition system for highly distributed particle detecting networks
S Chilingaryan, A Chilingarian, V Danielyan et al.

This content was downloaded from IP address 192.17.106.135 on 01/07/2026 at 23:25

ENVIRONMENTAL RESEARCH
LETTERS

Check for updates

OPEN ACCESS

RECEIVED
12 September 2025

REVISED
1 March 2026

ACCEPTED FOR PUBLICATION
17 June 2026

PUBLISHED
25 June 2026

Original content from this work may be used under the terms of the Creative Commons Attribution 4.0 licence.

Any further distribution of this work must maintain attribution to the author(s) and the title of the work, journal citation and DOI.

LETTER

Asymmetric urban–rural continuums (URCs) of Southeast Asian cities

Jin Wang[1], **Jiquan Chen**[1,*], **Peilei Fan**[2], **Soe W Myint**[3], **Zhenhai Liu**[1], **Jiaguo Qi**[1], **Atul K Jain**[4], **Karen Seto**[5] **and Yuanhui Zhu**[3]

[1] Center for Global Change and Earth Observations, Michigan State University, East Lansing, MI 48823, United States of America
[2] Department of Urban and Environmental Policy and Planning, Tufts University, Medford, MA 02155, United States of America
[3] Department of Geography and Environmental Studies, Texas State University, San Marcos, TX 78666, United States of America
[4] Department of Climate, Meteorology, and Atmospheric Sciences, University of Illinois, Urbana, IL 61801, United States of America
[5] Yale School of the Environment, Yale University, New Haven, CT 06511, United States of America
[*] Author to whom any correspondence should be addressed.

E-mail: jqchen@msu.edu

Keywords: landscape structure, urban–rural continuum, directional gradient analysis, asymmetry

Abstract

Conventional urban models are not always effective for addressing the unique spatial features. More recent remote sensing approaches also face difficulties in comprehensively generalizing the asymmetric nature of spatially complex urban–rural continuums (URCs). These areas are increasingly shaped by rapid urbanization and diverse natural conditions, resulting in highly asymmetric spatial structures. We aim to bridge this gap by comprehensively analyzing the asymmetric spatial characteristics of 19 cities across nine major Southeast Asian countries, highlighting the similarities and differences among the varying sized URCs. The proposed approach integrates a novel directional gradient-based method grounded in reliable land cover data, along with Windrose analysis, spatial statistics, and landscape indices. It quantitatively analyzes the key asymmetric characteristics of diverse URCs while covering only a limited area. Using this approach, we assessed the spatial asymmetry and variation of landscape diversity, urban density, and spatial morphology variation across and within these URCs. Results reveal that these URCs exhibit pronounced spatial asymmetry, which is shaped by natural features (e.g. rivers, terrain, coastlines, natural reserves) and artificial boundaries. The urban–rural fringe consistently shows the highest landscape diversity with an average Shannon Evenness Index of 0.87, much higher than that of urban center (0.32) or rural area (0.60). Directional asymmetry is further evidenced by the standard deviation (STD) of urban density by direction, which averages 0.11 across all cities. This asymmetry is particularly pronounced in coastal cities (average STD = 0.14), where coastlines strongly influence landscape configuration. Additionally, urban size also influences the degree of spatial asymmetry. The proposed analytical framework offers reliable data and practical tools for quantitatively analyzing asymmetry across diverse URCs. More crucially, it provides fundamental insights into urban structure that directly support urban planning and sustainable development.

1. Introduction

Urban areas have long been defined not only by their administrative or physical boundaries but also through the lens of the urban–rural continuums (URCs) that consider urban centers and their neighboring rural areas as a cohesive system (Schneider *et al* 2015, Zheng *et al* 2022). The URC has been often defined as dynamic spaces of socioeconomic interactions and exchanges (Skinner 2002, Cattaneo *et al* 2022). In the literature, URC is also referred to as the rural–urban continuum or the urban–rural interfaces (Pahl 1966, Karlsson 1986). In 1925, Burgess (1925) proposed the concentric zone model that conceptualizes cities as a series of concentric circles radiating outward from downtown to the suburbs. This conceptual framework was advanced through viewing urban areas as sectors (Hoyt 1939), or as multiple nuclei (Harris and Ullman 1945). While the concept is useful for studying URC, it remains mostly

© 2026 The Author(s). Published by IOP Publishing Ltd

abstract amid an increasing number of case studies (Schwirian 2007, Tian and Chen 2022). The complex spatial characteristics of modern cities, such as spatial differentiation and isolation problems, pose pressing challenges to these classical models (Fujii and Hartshorni 1995, Stokes and Seto 2019). Rapid urban growth, diverse natural conditions, and massive populations, render modern megacities too complex to be adequately explained through the direct application of these models (Schneider *et al* 2015, Zheng *et al* 2022).

Since 2000, numerous efforts have been made to investigate landscape features across URCs in different regions. Qi *et al* (2004) demonstrated the tightening link between urban centers and their peripheries during urban expansion. Weng and Lu (2009) applied a linear spectral unmixing model to analyze urban landscape structure and its dynamics. In Europe, Hedlund (2016) introduced a concentric framework to describe rural landscape typologies in Sweden, while Wilkosz-Mamcarczyk *et al* (2020) analyzed how urban expansion in Krakow, Poland, reshaped the surrounding URCs. Studies in Latin America similarly documented distinct gradients of landscape change, such as those observed across the URCs of Quito, Ecuador (Ortiz-Báez *et al* 2021). These studies illustrate that URCs are not simple linear transitions from urban to rural areas, but rather complex interfaces of heterogeneous surfaces (Vizzari *et al* 2018, Cattaneo *et al* 2022). Furthermore, various levels of urban development leave distinct footprints on the landscape across URCs (Hedlund 2016, Cattaneo *et al* 2022, Fan *et al* 2022, Tian and Chen 2022). The resulting spatial asymmetry in urban areas not only reshapes community structures but also creates ecological gradients and edge effects that influence the movement of water, nutrients, and organisms across the landscape (Cumming *et al* 2008). It also intensifies thermal variations, contributing to urban heat-related effects (Zhao *et al* 2025, Cao *et al* 2026).

Based on our synthesis of URC studies (table 1), quantitative analysis of asymmetric landscape structures remains largely unexplored (Peng *et al* 2018). Understanding and quantifying the landscape asymmetry of cities requires thorough exploration beyond qualitative or conceptual interpretations (Phiri *et al* 2020, Li *et al* 2023). There is an obvious knowledge gap regarding the differences and similarities in urban asymmetry across cities of varying sizes (Gluch and Ridd 2010, Peng *et al* 2018). It is also unclear how asymmetry is shaped by different geographic or institutional factors, such as centralized planning versus market-driven governance, and intensified development versus conservation efforts (Chen *et al* 2018, Fan *et al* 2019).

To address this knowledge gap, this study aims to examine the asymmetric nature of the 19 cities in Southeast Asia (SEA) (Nguyen *et al* 2025, Zhu *et al* 2025). In recent years, SEA has emerged as a key global region with robust economic growth far exceeding the global average (Fan *et al* 2022, HSBC 2024, IMF 2024). Covering 3.1% of the world's land, SEA is home to 8.9% of the global population, or 700 million people, of whom 52.8% lives in urban areas (UN Population Division 2024). Decades of rapid and continuous urbanization in SEA have driven significant environmental changes and reshaping landscape structures not only within urban areas but also across the extended fringes and rural regions that interface with urban centers (Sarker *et al* 2024a, Zhu *et al* 2025). Since URC has been successfully applied to analyze complex interfaces shaped by multiple anthropogenic and natural drivers, we use this term to define the broader study area of the 19 SEA cities rather than merely focus on the urban area. We hypothesize that urban and natural landscapes within these URCs in SEA exhibit significant, quantifiable asymmetry that deviates from idealized conventional urban models. Since gradient analysis can reduce subjectivity and enhance reproducibility in spatial studies (Vizzari and Sigura 2015, Ortiz-Báez *et al* 2021), we propose an analytical framework based on a directional gradient to model the asymmetric URCs.

The specific objectives of this study are to: (1) develop a novel, intuitive, and transformative framework for studying URC asymmetry, taking 19 SEA cities as our testbed; and (2) synthesize the similarities and differences among these URCs through quantitative directional gradient analysis. Through this framework, we aim to reveal the asymmetric nature of these landscapes, deepening the understanding of URCs with diverse structures and complex environments while informing urban development and planning.

2. Materials and methods

2.1. Study area

We selected 19 studied cities across nine major SEA countries (figure 1, table 2). Aimed at capturing the diversity of urban typologies, the studied cities include capitals or former capitals, regional economic centers, and municipalities of varying sizes (Zhu *et al* 2025). Crucially, these cities provide a balanced representation of key geographic conditions: 10 are coastal while 9 are inland; 13 are situated in Mainland SEA, and 6 in the Malay Archipelago. This diversity facilitates a comprehensive and comparative analysis of how different natural and administrative contexts shape landscape structures. Although these 19 URCs cover only 5.42% of SEA's terrestrial area, they have a population of 186.88 million, or 28.61% of the total in the SEA area.

In this study, the centers of the selected cities were defined based on the geocoded coordinates of Google Maps (table 2). These locations typically align

Table 1. Summary of representative studies and theoretical developments on urban–rural continuum (URC).

Period	Key Authors	Approach/model	Contribution/insight
Prior to 1960	Burgess (1925), Hoyt (1939), and Harris and Ullman (1945)	Concentric zone, Sector, and multiple Nuclei model	Proposed early systematic model of urban spatial structure.
1960–2000	Pahl (1966), Karlsson (1986), and Bell (1992)	Urban–rural Continuum (urban–rural interfaces/rural–urban continuum)	Conceptualized cities and surrounding rural areas as continuous and interacting systems rather than distinct zones
2000–2015	Qi *et al* (2004), Weng and Lu (2009)	RS-Based URC study	Quantitatively analyzed urban landscape structure and its temporal changes using remote sensing.
2008–Present	Cumming *et al* (2008), Wilkosz-Mamcarczyk *et al* (2020), Zhao *et al* (2025), Cao *et al* (2026)	Spatial landscape study with socioecological analysis	Highlighted URCs as complex interfaces shaped by multiple anthropogenic and natural forcing.
2015–Present	Hedlund (2016), Vizzari *et al* (2018), Fan *et al* (2019), Ortiz-Báez *et al* (2021), Cattaneo *et al* (2022), and Tian and Chen (2022)	Multisource data integration	Emphasized the use of advanced high-resolution and multisource geospatial data to quantify urban structure, expansion, and environmental effects.

with administrative landmarks or historic cores, serving as standardized, functional starting points for directional landscape analysis. Compared with mathematical centroid methods, the labels of Google Maps provide a more stable representation of the functional city centers. A detailed comparison with the alternative city center determination approaches is provided in appendix A. To comprehensively study these landscapes across the extended fringes and rural areas that interface with the urban center, URCs were delineated using a 5 km buffer zone of each city's municipal administrative boundaries. The population was estimated based on the 2023 LandScan gridded population dataset (Lebakula *et al* 2024). The 19 studied URCs were categorized into three groups based on the physical extent of their continuous urban areas. Specifically, URCs with urban areas extending beyond 20 km were classified as large cities, those between 10–20 km as medium, and those under 10 km as small (table 2). The urban areas classification is directly derived from the directional gradient analysis in section 3.2.

2.2. Data and pre-processing

We applied the land use/land cover of 2023, derived from Sentinel-2 image (10 m resolution) by ESRI using deep learning AI model (ESRI 2024). The land cover products were adjusted based on the International Geosphere-Biosphere Programme classification system consists of nine classes: Forests, Grasslands, Wetlands, Built-up lands, Croplands, Barren, Water bodies, Snow & ice, and Clouds (Loveland and Belward 1997). QuickBird images (0.6 m), covering limited areas were acquired to support accuracy assessment and detailed analysis. The accuracy assessment yielded an overall accuracy of 81.8% for the nine land cover classes and 85.0% for the four aggregated landscape categories.

2.3. Methods

A directional gradient analysis was performed to explore the configuration and diversity of landscape (figure 2). Specifically, circular zones at 1 km intervals from city center were generated, extending to the boundaries of the URCs. This approach has proven effective in gradient analyses from recent urban studies (Wang *et al* 2020, Zheng *et al* 2023, Sarker *et al* 2024a). Our preliminary assessment further confirms that 1 km is an appropriate scale for characterizing urban land surfaces, avoiding oversmoothed patterns while preserving sensitivity to directional gradient changes (Barnes *et al* 2002, Jiao 2015). The gradient analysis was performed along the grids in eight cardinal and diagonal directions for exploring the asymmetric nature of the landscapes. The original land cover classes were aggregated into four landscape categories: Urban area (built-up lands), Semi-natural surface (cropland, barren, and grasslands), Natural surface (forests, wetlands, and the others), and Water bodies, with reference to previous studies (Zorrilla-Miras *et al* 2014, Jiao 2015). The dominant landscape category of each grid was identified. Urban density was then calculated by determining the proportion of urban area within each grid.

Sample standard deviation (STD_s) of urban density was calculated for assessing the variability of urban density with distance and by direction (table 3). The population standard deviation (STD_p)



Figure 1. Spatial distribution of the 19 study cities in nine countries of Southeast Asia (SEA). The unshaded areas indicate the administrative land areas of the study cities.

was computed for the mean urban densities across all eight directions to evaluate directional variations in urban density. This measure captures the extent of asymmetry in urban development, highlighting whether certain directions exhibit significantly higher or lower urban densities compared to others. A higher STD_p value signifies pronounced directional variations.

Four quantitative metrics on landscape asymmetry were calculated (table 3). The Shannon Evenness Index (SHEI) of landscape categories across each URC zones (Urban Center, Urban Fringe, and Rural Area) was calculated to assess the asymmetry of landscape structure. SHEI is a key index that measures LULC diversity based on the number of landscape classes in an area (Shannon 1948). It is computed by dividing the Shannon Diversity Index (SHDI) by the natural logarithm of the number of categories. Therefore, SHEI is calculated as the fraction of the observed SHDI to the maximum possible SHDI (Kodl *et al* 2024). This normalization remarkably reduces the influence of the total category count. Unlike SHDI which does not have a fixed value range, SHEI ranges from 0 to 1 regardless of category count. An SHEI value of 1 indicates perfectly even proportions among landscape categories, while values approaching 0 indicate dominance by a single category (ORNL, & NASA 2019).

Table 2. Basic information about the 19 study cities and associated urban–rural continuums (URCs) in Southeast Asia (SEA). References: Google Maps and LandScan Silver Edition (https://doi.org/10.48690/1531770).

Type of city	Name	Country	City center	City center coordinates	Urban extent (km)	URC area (km^2)	Population (2023)	Description
Large	Ho Chi Minh City	Vietnam	Giac Lam Buddhist Temple	10°49.39′ N, 106°37.78′ E	81	35 905	24.63 m	Vietnam's most populous city and economic center, a centrally controlled municipality.
	Hanoi	Vietnam	Temple of literature	21°1.67′ N, 105°50.05′ E	65	29 569	22.68 m	Capital and second most populous city of Vietnam.
	Bangkok	Thailand	Democracy Monument	13°45.38′ N, 100°30.11′ E	35	9919	17.23 m	Capital and most populous city of Thailand.
	Jakarta	Indonesia	Selamat Datang Monument	6°11.67′ S, 106°49.38′ E	39	9000	34.68 m	Capital and most populous city of Indonesia.
	Manila	Philippines	Quiapo church	14°35.97′ N, 120°59.05′ E	26	10 943	31.05 m	Capital and most populous city of Philippines.
	Kuala Lumpur	Malaysia	Independence square	3°8.97′ N, 101°41.67′ E	29	10 981	10.14 m	Capital and most populous city of Malaysia.
Medium	Bandung	Indonesia	Kebon Pisang district	6°55.05′ S, 107°37.15′ E	17	6985	11.52 m	Capital of West Java province; fourth most populous city in Indonesia.
	Yangon	Myanmar	Center Wai Za Yan Tar Rd	16°50.46′ N, 96°10.41′ E	14	12 223	8.86 m	Most populous city and former capital of Myanmar.
	Chiang Mai	Thailand	Wat Chai Phrakiat temple	18°47.30′ N, 98°59.12′ E	19	31 862	2.14 m	Capital of Chiang Mai Province, second most populous city in Thailand.
	Phnom Penh	Cambodia	Independence Monument	11°33.38′ N, 104°55.69′ E	14	5820	4.33 m	Capital and most populous city of Cambodia.
	Vientiane	Laos	Thatluang grounds	17°58.54′ N, 102°37.99′ E	17	5392	1.21 m	Capital and most populous city of Laos.
	Singapore	Singapore	CapitaGreen tower	1°16.87′ N, 103°51.02′ E	17	1594	6.16 m	Island city-state and economic center of SEA.
Small	Denpasar	Indonesia	Dauh Puri Klod Commercial district	8°40.23′ S, 115°12.77′ E	8	1514	1.93 m	Capital of Bali province.
	Johor Bahru	Malaysia	Plaza Pelangi	1°28.79′ N, 103°45.86′ E	10	1703	1.96 m	Capital of Johor state; adjacent to Singapore.
	Siem Reap	Cambodia	Sokha Angkor resort	13°21.80′ N, 103°51.38′ E	6	13 104	1.22 m	Second most populous city of Cambodia; gateway to Angkor Wat.
	Chiang Rai	Thailand	King Mangrai Monument	19°54.63′ N, 99°50.43′ E	7	13 821	1.38 m	Capital of Chiang Rai Province, near Laos and Myanmar borders.
	Iloilo	Philippines	SM Hypermarket Iloilo	10°43.21′ N, 122°33.73′ E	6	9353	3.10 m	Capital of Iloilo Province, Philippines.
	Pakse	Laos	Champasack Stadium	15°7.03′ N, 105°48.95′ E	3	18 982	0.96 m	Capital of Champasak Province; the confluence of the Mekong and Xe Don rivers.
	Naypyidaw	Myanmar	Wunna Theikdi stadium	19°45.80′ N, 96°4.71′ E	3	12 017	1.70 m	Current capital and third most populous city of Myanmar.

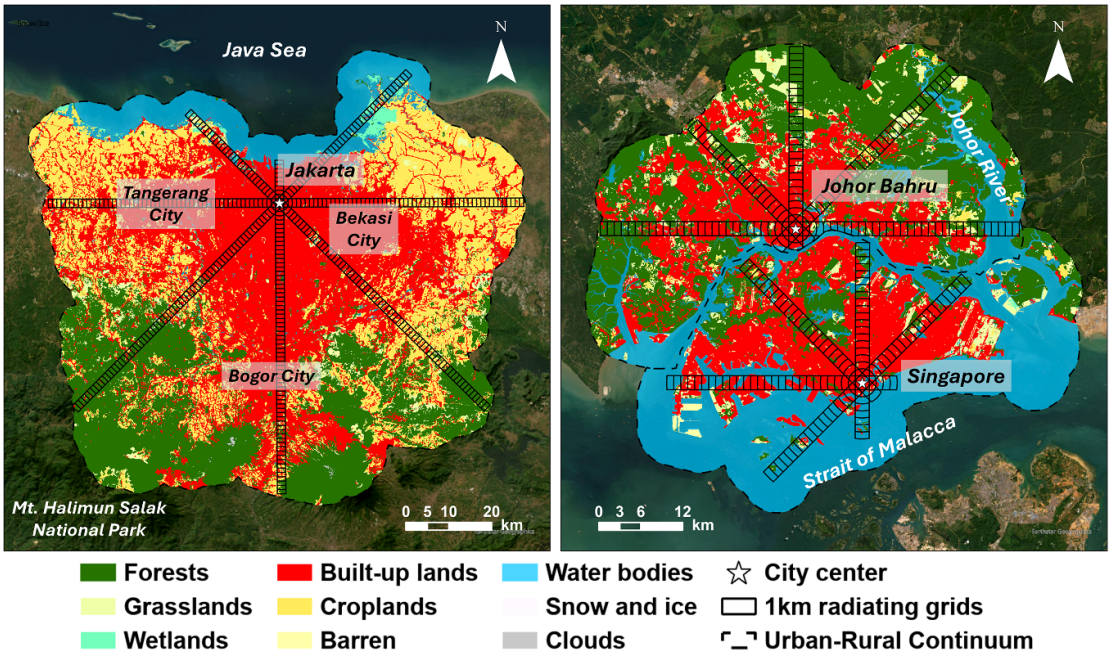


Figure 2. Illustrations of extracting landscape features from city centers to rural areas at 1 km intervals in 8 directions for exploring the asymmetry of urban–rural continuums (URCs). Jakarta (left) represents a large city, while Singapore and Johor Bahru (right) represent medium and small cities, respectively. The detected secondary urban centers of Jakarta (e.g. Tangerang, Bekasi, Bogor) are labeled. The land use/land cover maps of 2023 derived from the Sentinel-2 images (10 m resolution) by ESRI are used as examples for changes in land cover types along the URCs.

Table 3. Four quantitative metrics and their definitions for quantifying the asymmetry among the 8 directional URCs in 19 study cities in Southeast Asia. Sample standard deviation (STD_s) and population standard deviation (STD_p) are used to quantify directional urban density variations within each URC, while Shannon Diversity Index (SHDI) and Shannon Evenness Index (SHEI) measure landscape heterogeneity.

Spatial index	Equation	Variable definitions
Sample standard Deviation	$STD_s = \sqrt{\frac{1}{7}\sum_{i=1}^{8}(d_i - \bar{d})^2}$	d_i: urban density in the ith direction at a given distance (m) $\bar{d}$: mean urban density at a given distance
Population standard deviation	$STD_p = \sqrt{\frac{1}{8}\sum_{i=1}^{8}(D_i - \bar{D})^2}$	D_i: mean urban density in the ith direction $\bar{D}$: average urban density among all directions
Shannon Diversity Index	$SHDI = -\sum_{i=1}^{m}(P_i * \ln P_i)$	P_i: the proportion of the landscape occupied by category i
Shannon Evenness Index	$SHEI = \frac{SHDI}{\ln m}$	m: the number of landscape categories

3. Results

3.1. Urban landscape and morphology

Directional gradient analysis of landscape categories reveals that the URCs are asymmetric but differ substantially from each other (figures 3 and 4). The Windrose diagrams not only provide city-specific visualization of directional growth, but also enable cross-case synthesis of how landscape composition diverges across urban, semi-natural, and natural surfaces.

First, larger cities exhibit broader and more continuous urban petals, reflecting a stronger expanded pattern. For example, the urban area of Ho Chi Minh City (HCMC) is approximately ten times larger than that of Naypyidaw. Second, the degree and orientation of asymmetry are consistently shaped by physical geography and political boundaries. While many cities display a typical concentric pattern from urban to semi-natural to natural surfaces, others show distinctive configurations. For instance, Kuala Lumpur, Singapore, and Johor Bahru have minimal semi-

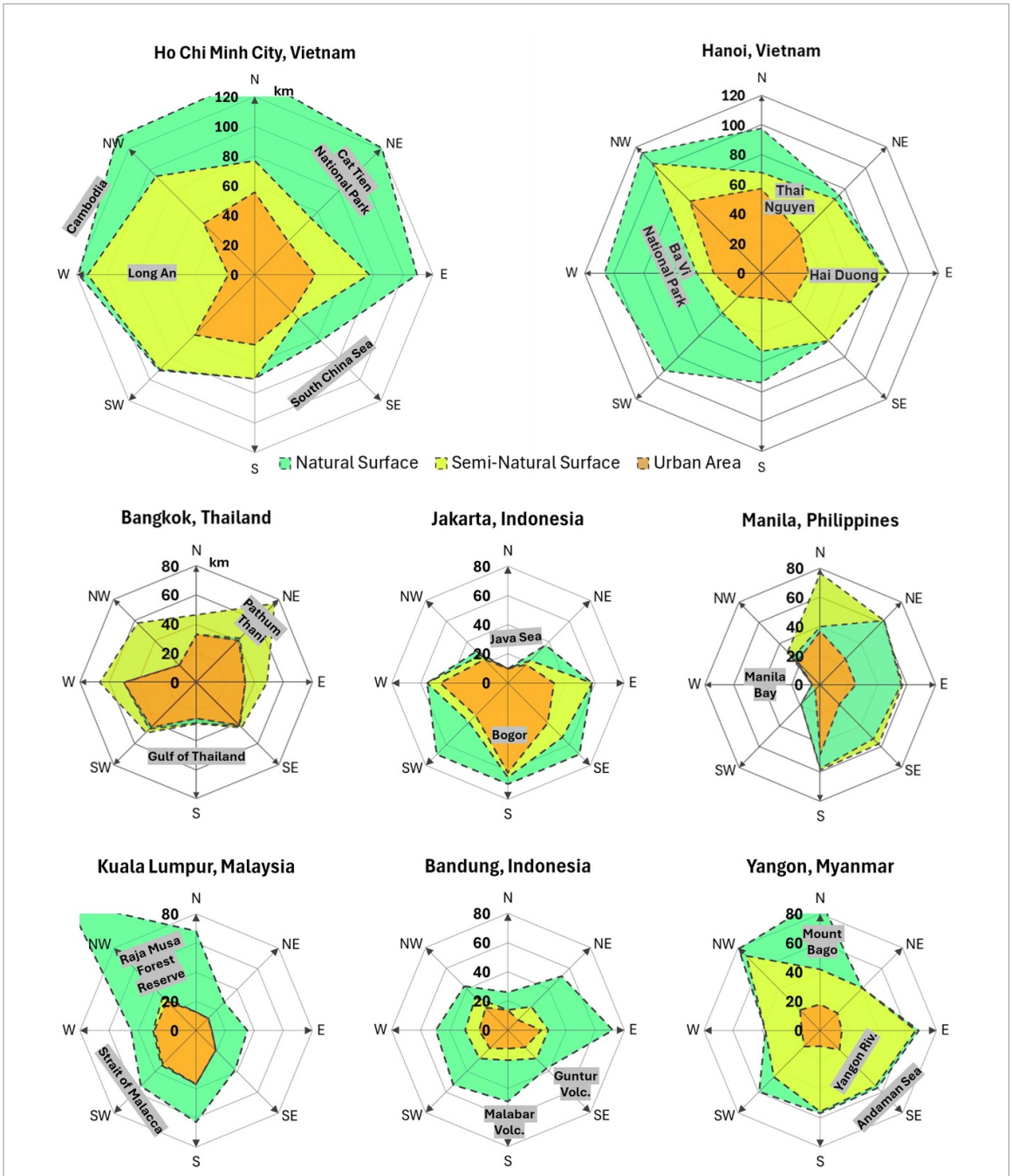


Figure 3. Windrose diagrams illustrating the directional characteristics of dominant landscape categories (urban, semi-natural, and natural) within the URCs of SEA (large and medium cities). Each Windrose is generated based on directional gradient grids extending from the city center in eight directions (north, northeast, east, southeast, south, southwest, west, northwest). The length of each petal represents the extent of the dominant landscape category in that direction, providing a visual assessment of the spatial heterogeneity and asymmetry in landscape composition. Important natural features and artificial boundaries that influence urban structure are labelled on each Windrose. Abbreviations: Volc. (volcano); Riv. (river).

natural surfaces because natural and artificial barriers restrict arable land, resulting in an abrupt transition from urban to natural cover. Conversely, cities like Bangkok lack substantial natural surfaces, as agricultural land dominates the areas beyond its urban core. Additionally, coastal cities show more pronounced asymmetry in their landscape structure, as growth is truncated in directions facing the sea.

Both physical geography and administrative boundaries strongly influence the URCs' asymmetry. In most cases, urban areas and semi-natural surfaces are constrained by natural features, as well as by artificial boundaries such as national borders. These features produce shorter petals for urban and semi-natural surfaces in the Windrose diagrams, while simultaneously directing growth toward less constrained sectors and creating distinct asymmetry (figures 3 and 4). For instance, a major river or mountain range on one side of a city will halt development there, forcing expansion along other directions. Similarly, for many URCs adjacent to national borders, large areas

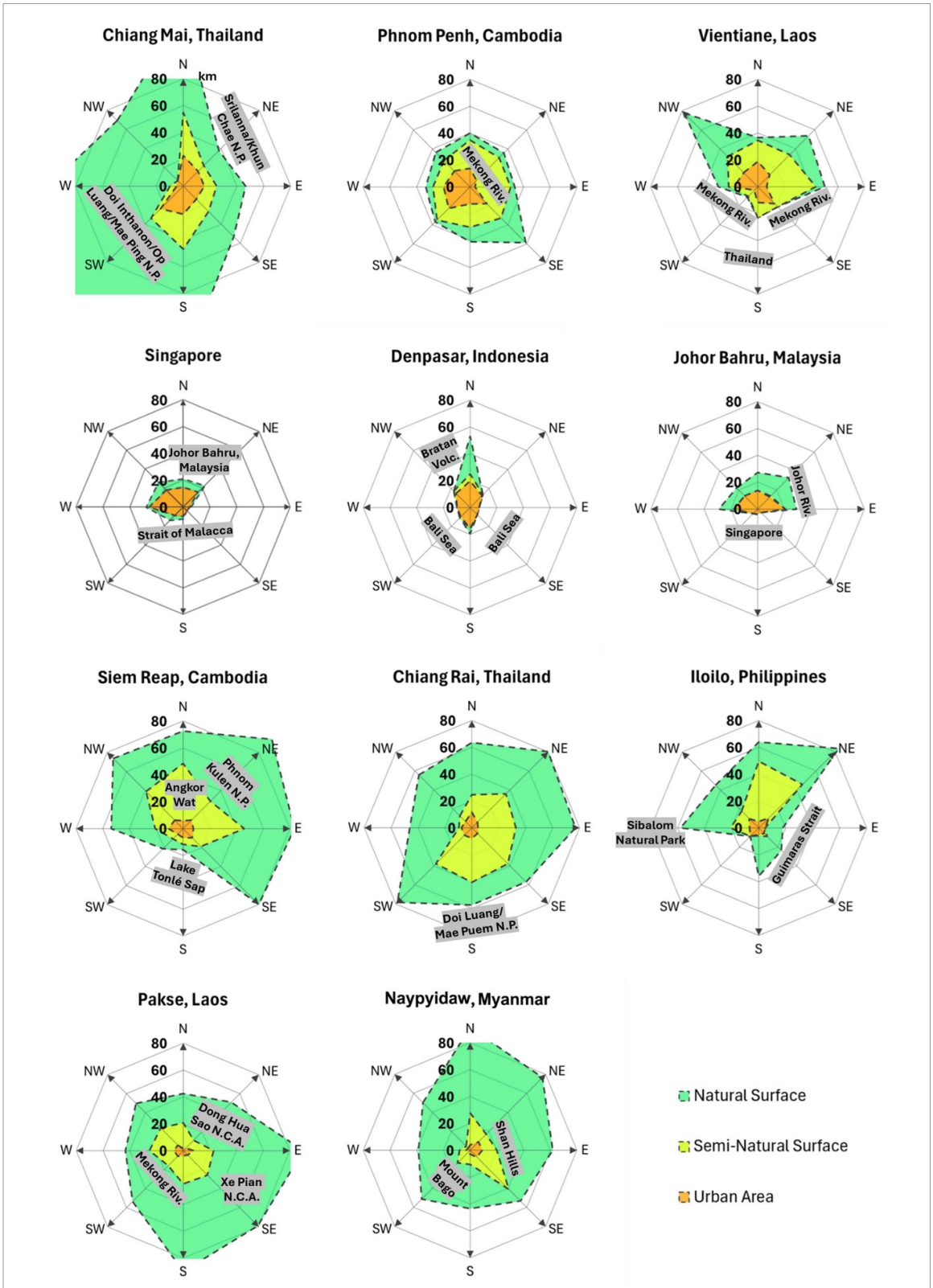


Figure 4. Windrose diagrams illustrating the directional characteristics of landscape features (urban, semi-natural, and natural) within the URCs of SEA (medium and small cities). Petal lengths indicate the extent of dominant landscape features (urban, semi-natural, natural) in each of the eight directions, i.e. the asymmetric nature of landscape composition. Selected critical natural and man-made landmarks for each city are labeled. Abbreviations: N.P. (National Park); Riv. (river);Volc. (volcano); N.C.A. (National Conservation Area).

of natural surface occupy the space between the border and the city center, further contributing to the asymmetric landscape composition of the URCs.

Landscape diversity peaks at the urban fringe. The diversity and evenness of land cover composition vary systematically from urban center to rural area, generally peaking in the intermediate urban fringe. To

Table 4. Average Shannon Evenness Index (SHEI) in urban centers, urban fringes, and rural areas across the urban–rural continuums (URCs) of 19 study cities in SEA. High SHEI values approaching 1 indicate increasingly even proportions among the eight directions of a landscape feature, while values approaching 0 signify increasingly uneven distributions by direction.

City	Urban center	Urban fringe	Rural	Total radian area	Overall URC
Ho Chi Minh City	0.30	0.87	0.76	0.98	0.97
Hanoi	0.38	0.88	0.56	1.00	0.95
Bangkok	0.24	0.84	0.59	0.93	0.97
Jakarta	0.22	0.85	0.78	0.88	0.99
Manila	0.32	0.96	0.77	0.93	0.81
Kuala Lumpur	0.45	0.72	0.39	0.76	0.71
Bandung	0.27	0.85	0.32	0.96	0.94
Yangon	0.26	0.91	0.68	0.91	0.80
Chiang Mai	0.29	0.82	0.47	0.90	0.71
Phnom Penh	0.33	0.93	0.73	0.97	0.87
Vientiane	0.32	0.93	0.65	1.00	0.90
Singapore	0.37	0.83	0.43	0.76	0.70
Denpasar	0.20	0.95	0.63	0.89	0.90
Johor Bahru	0.36	0.83	0.51	0.91	0.80
Siem Reap	0.20	0.82	0.75	0.85	0.71
Chiang Rai	0.36	0.75	0.48	0.87	0.78
Iloilo	0.28	0.92	0.81	0.83	0.70
Pakse	0.43	0.96	0.53	0.78	0.68
Naypyidaw	0.53	0.86	0.54	0.78	0.74

quantify the gradients, each URC was segmented into three zones: urban center, urban fringe, and rural area. Consistent with Peng *et al* (2018), the segmentation was determined by the proportion of built-up land within each grid. Based on the thresholds established in previous studies (Lu and Weng 2006, Van de Voorde *et al* 2011), grids with a built-up density of >80% were classified as urban centers, which are dominated by continuous commercial and residential areas. Grids with values between 20% and 80% were defined as the urban fringe, characterized by medium-intensity industrial or discontinuous residential areas, while those with <20% were classified as rural areas, mainly consisting of non-urban surfaces such as extensive vegetation and agricultural lands. Based on the asymmetry quantification (table 4), we found that most of the URCs' urban fringes had an SHEI value of > 0.8, reflecting a heterogeneous mix of different land categories. In contrast, the urban centers had the lowest SHEI values, often <0.4, as they were overwhelmingly dominated by built-up lands. The SHEI values of rural areas normally fall between those of the urban centers and fringes.

Additionally, larger cities tend to have higher overall SHEI than smaller ones (table 4). HCMC, Bangkok, and Jakarta show the highest overall SHEI values, indicating more complex landscape composition. In contrast, smaller cities often have lower overall SHEI values of around 0.7–0.8, implying less heterogeneous landscape categories within their URCs. Furthermore, analyses of the radian area yield results similar to those for the overall URCs, suggesting that the radian areas are effective samples for comprehensive analysis with significantly reduced data and computation.

3.2. Asymmetric urban density across URCs

Large cities maintain high urban density extending far beyond their centers, whereas smaller cities show sharp declines over shorter distances. Figure 5 summarizes these variations by boxplots of urban density at 1 km intervals along eight directions, with the solid line indicating the mean density. Spatially, urban density across the 19 URCs generally decreases with distance from the city core. It tends to decline gradually within the urban center, drop sharply at the transition to urban fringe, and decrease slowly in rural areas. As city size increases, both the intensity and spatial extent of urban density broaden, while the center-rural gradient becomes more gradual. Still, the differences among cities are pronounced, highlighting the inherent asymmetry in urban density patterns. For most large cities, urban centers with densities exceeding 0.8 typically extend to 10 km from the city core. However, Bangkok's urban center reaches beyond 20 km, whereas Manila's extends to only about 5 km. The spatial extent of urban fringe areas, characterized by densities of 0.2–0.8, also varies considerably among the large cities. For instance, the urban fringes of HCMC and Hanoi reach 70–80 km, while in other large cities urban fringe areas transition to rural landscapes at ∼40 km. Medium cities experience a rapid decline in urban density within 10 km of their centers. Their urban fringe zones often extend up to 20 km. Small cities typically have limited urban centers and urban fringes that span no more than 5 km, respectively, and rural areas dominate the areas beyond

10 km from the city center. Further analysis based on the Standard Deviation of urban density across eight directions confirms that directional differences peak at the urban fringe, whose size varies at different city scales (appendices B and C).

All six large cities contain secondary urban centers within their URCs, while all medium and small cities maintain monocentric urban structure (figure 5). A secondary urban center is defined when all three conditions are met: (1) it must be located beyond 20 km from the primary city-center point (the extent of the main urban center in large cities); (2) it must include grids with built-up density greater than 80%, consistent with the threshold for defining a main urban center; and (3) it must extend continuously at least 5 km, equivalent to the extent of a main center in small cities. Among all nine detected secondary centers, seven are located within 30 km of the primary center. However, located 61 km north of the city center of Hanoi, Thai Nguyen represents the farthest secondary center identified in this study. Thai Nguyen is itself a first-class provincial city in Vietnam. Jakarta contains three secondary centers (Tangerang to the west, Bekasi to the east, and Bogor to the south), the most among all studied cities. Among them, Bogor is the farthest, located 38 km from Jakarta's center.

Coastal cities exhibit pronounced directional variation of urban density. Ranging from 0.03 to 0.22, the STD_p of urban density across different directions reflects a wide range of spatial variations from balanced to asymmetric (table 5). The cities with the highest STD_p values, specifically Singapore, Johor Bahru, Manila, and Denpasar, are all coastal. Their coastlines strongly influence urban structures and constrain development in directions towards their coasts. For instance, in Singapore urban density is high toward the north and west (>50%) but drops sharply toward the east and south due to the Singapore Strait. Similarly, Manila's density is significantly lower in the southwest, where Manila Bay restricts expansion. In contrast, many inland cities demonstrate lower directional variation. Small cities such as Chiang Rai, Pakse, and Naypyidaw all have STD_p values of <0.05, indicating relatively even urban development in all directions. The small cities' urban centers are less developed and have not yet expanded to reach the major natural barriers within their URCs, allowing current urban expansion to proceed more uniformly. Larger inland cities like Hanoi, Chiang Mai, and Bandung show moderately higher STD_p values (0.07–0.10), reflecting asymmetry but still less than the coastal cities. Exceptions do exist among inland cities such as Vientiane and Phnom Penh, which display considerable directional variation ($STD_p = 0.15$), likely shaped by rivers, terrain, national borders, and infrastructure corridors that guide expansion along preferred axes. These findings suggest that in addition to coastlines, other geographic and infrastructural elements also contribute to landscape asymmetry.

Cities with broad, open plains tend to exhibit more symmetric spatial patterns. Hanoi, Bangkok, and Yangon have the lowest STD_p among the large and medium cities, all less than 0.10 (table 5). The broad alluvial plains characterizing these URCs allow the urban surface to develop into compact and concentric forms, resulting in a spatially uniform structure across all directions. In addition, Bangkok's coastline is comparatively straight, which reduces directional constraints and contributes to its lower degree of asymmetry relative to other coastal cities.

National borders also play an important role in shaping asymmetry. Directions leading from the city center toward an international border can have the lowest urban density of all directions. This is evident in HCMC (westward toward Cambodia), Chiang Rai (northeastward toward Laos), and Pakse (southward toward Cambodia), as indicated by the underlined values in table 5. Interestingly, the opposite trend also occurs in border cities such as Vientiane, Singapore, and Johor Bahru, where the directions toward Thailand, Malaysia, and Singapore, respectively, exhibit the highest urban densities. This seemingly paradoxical phenomenon can be explained by differences in neighboring countries' economic development: urban area can expand toward borders shared with more developed countries, while it can also expand away from borders shared with less developed neighbors. Both ways contribute to the asymmetric structure of URCs. In addition, population density also significantly influences the degree of directional asymmetry, as detailed in appendix D.

4. Discussion

In this research, we utilized directional gradient grids to quantify the landscape asymmetry rather than examine the entire URC area. Dai *et al* (2018) concluded that gradient analysis effectively captures the continuous directional changes in landscape heterogeneity. A related comparative study of Bangkok, HCMC, and Manila based on concentric rings shows that coastal cities like Manila are significantly constrained by coastlines, resulting in asymmetric landscape structures (Xu *et al* 2019). These findings align closely with the results of this study, which indicate that coastal cities exhibit the highest directional variability (table 5). This demonstrates that the directional gradient can quantitatively analyze asymmetric landscape structures commensurable to full-extent analysis, but with substantially reduced data requirements.

Challenges could arise when applying this method to modern large cities with secondary urban centers. Intuitively, analysis based on directional gradient

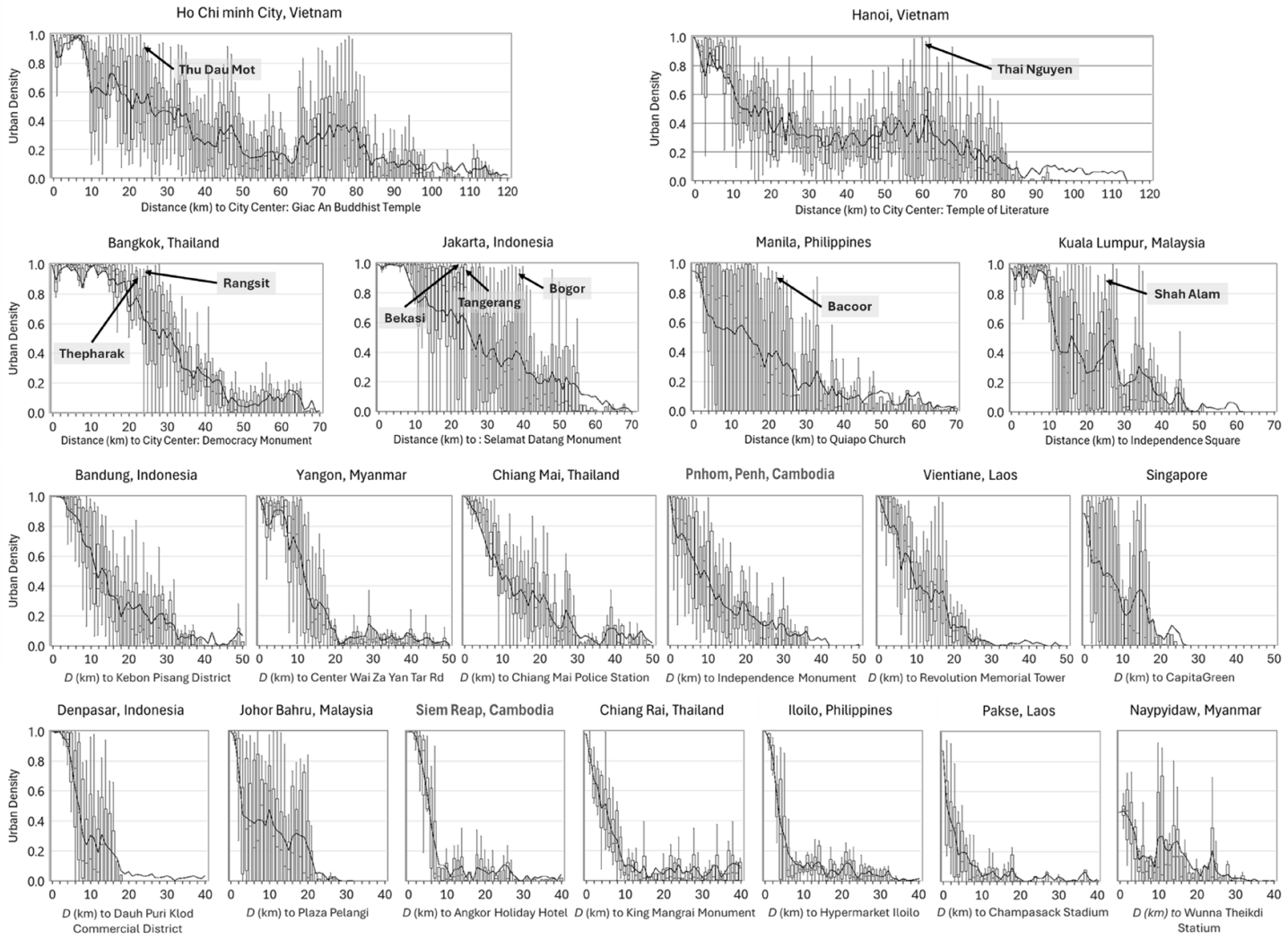


Figure 5. The boxplots of the changes in urban density from the city center to rural landscapes (i.e. the 19 urban–rural continuums, URCs) at 1 km intervals in 2023. The mean and variation at a given distance are calculated using data from eight directions (figure 1). Urban density is calculated as the proportion of urban area within each 1 km grid cell to the total land area. Secondary urban centers identified within the URCs are labeled on the corresponding plots, indicating their specific distances and urban density values. Note that the maximum distance for small, medium, and large cities was set at 40 km, 50 km and 70 km, respectively.

Table 5. The average urban density in the eight directions and the corresponding population standard deviation (STD_p). The directional averages highlight the asymmetry of urban density; STD_p indicates the overall degree of variability by direction. Underlined values mark the directions toward international borders that show either the lowest or highest density for the corresponding city.

City	Type	Average urban density (%)									STD_p
		Total area	N	NE	E	SE	S	SW	W	NW	
Ho Chi Minh City	Coastal	37.05	40.85	25.00	36.24	30.54	55.75	53.97	23.29	35.02	0.11
Hanoi	Inland	39.70	47.50	43.91	40.26	49.99	28.63	28.09	28.31	45.73	0.09
Bangkok	Coastal	59.98	66.70	55.57	69.21	62.41	56.71	60.41	54.30	44.75	0.07
Jakarta	Coastal	61.38	56.21	34.68	58.73	51.64	81.61	46.31	80.16	55.21	0.15
Manila	Coastal	35.59	50.36	39.11	44.39	20.24	61.98	5.04	37.24	16.50	0.18
Kuala Lumpur	Coastal	38.66	19.93	41.87	33.06	53.04	48.73	56.85	56.18	18.42	0.15
Bandung	Inland	37.64	47.69	22.20	31.76	47.04	27.01	36.61	37.23	52.07	0.10
Yangon	Coastal	24.19	20.10	38.88	21.10	25.71	17.15	21.29	27.04	24.45	0.06
Chiang Mai	Inland	17.93	18.67	29.76	32.25	29.06	17.03	14.45	7.13	10.23	0.09
Phnom Penh	Inland	34.20	29.26	18.20	15.44	23.05	25.84	58.02	55.37	41.66	0.15
Vientiane	Inland	34.48	44.89	21.60	22.68	66.68	55.79	43.56	45.79	18.38	0.16
Singapore	Coastal	44.64	66.32	56.83	8.58	20.62	18.01	19.57	54.32	64.48	0.22
Denpasar	Coastal	52.87	40.75	82.55	51.22	51.35	44.48	27.33	50.35	75.22	0.17
Johor Bahru	Coastal	56.79	44.47	35.17	45.54	80.80	87.47	88.00	55.47	64.76	0.19
Siem Reap	Inland	14.08	9.11	10.57	15.10	10.64	30.92	23.57	15.98	13.69	0.07
Chiang Rai	Inland	14.15	19.05	8.97	11.17	12.42	16.31	16.50	13.27	13.10	0.03
Iloilo	Coastal	15.39	15.23	8.53	20.47	15.47	12.11	43.50	15.25	20.86	0.10
Pakse	Inland	7.21	8.36	7.56	7.13	7.07	3.10	6.97	10.03	12.58	0.03
Naypyidaw	Inland	11.59	6.60	14.92	17.16	17.71	12.82	7.15	6.94	5.61	0.05

grids from a single center may be more suitable for traditional monocentric cities. But our examination indicates that the directional gradient grid analysis effectively captures and illustrates the asymmetric landscape structures of large, multicentric cities such as HCMC and Bangkok. Figure 6 further shows land cover maps overlaid with directional gradient grids for two large cities, HCMC (left) and Bangkok (right), along with their landscape structures illustrated by Windrose charts. As regional economic centers, both cities have multiple urban centers. In HCMC, in addition to the traditional center area around Giac Lam Buddhist Temple, which was chosen as the center of the directional gradient grids, District 7 has emerged as a dynamic, newly constructed CBD characterized by upscale amenities. Located relatively close to the traditional center, District 7 is precisely captured by the directional gradient analysis, illustrating southeastward urban expansion consistent with the HCMC's 2010 Master Plan (Downes *et al* 2024, Prime Minister of Vietnam 2025). Our analysis also identifies Thu Dau Mot as a secondary urban center of HCMC. Like Thai Nguyen, Thu Dau Mot is also one of Vietnam's 21 first-class provincial cities and has experienced rapid economic development. As shown in figure 6, the urban area extends towards the north and northwest of HCMC's URC, along with a series of southwestern satellite towns, which are also mostly covered by directional gradient grids. The Windrose-illustrated asymmetric landscape structure is consistent with the land cover map, indicating that the western part of HCMC's URC is dominated by crop areas in Long An province, and the northeastern part is dominated by forests in Cat Tien National Park.

Bangkok is a densely built-up capital city where transportation systems significantly influence the landscape structure (Vichiensan *et al* 2022, Sarker *et al* 2024b). However, unlike in HCMC, the directional gradient grids did not land in major satellite towns such as Rangsit and Nakhon Pathom (figure 6). Still, our analysis successfully detected Rangsit as a secondary urban center within the Bangkok URC (figures 5 and 6). Situated approximately 30 km north of the capital at the terminus of the SRT Dark Red Line, Rangsit facilitates direct connectivity to the traditional city center for its 100 000 residents (Boongla *et al* 2021). As the capital's northern gateway, this residential, educational, and commercial hub complements the capital. Although gradient grids did not land exactly on Rangsit, the Windrose chart nevertheless effectively depicts that urban areas dominate the north- and northeast-bound grids at ∼40 km from the center. This identified asymmetric landscape structure in the northeastern part of Bangkok's URC aligns closely with the land cover map of the entire URC. Similarly, though the western-bound gradient grids do not encompass Nakhon Pathom city, a historical and cultural center about 50 km west of Bangkok, the Windrose chart still accurately demonstrates that urban-dominated landscapes extend to that range. Furthermore, the land cover map indicates that the northwest part of Bangkok's URC is predominantly agricultural, which is corroborated by the Windrose chart showing that semi-natural surfaces dominate the northwest-bound gradient grids beyond 17 km from the urban center.

Many smaller cities retain a concentric structure, where urban density is highest at the center and

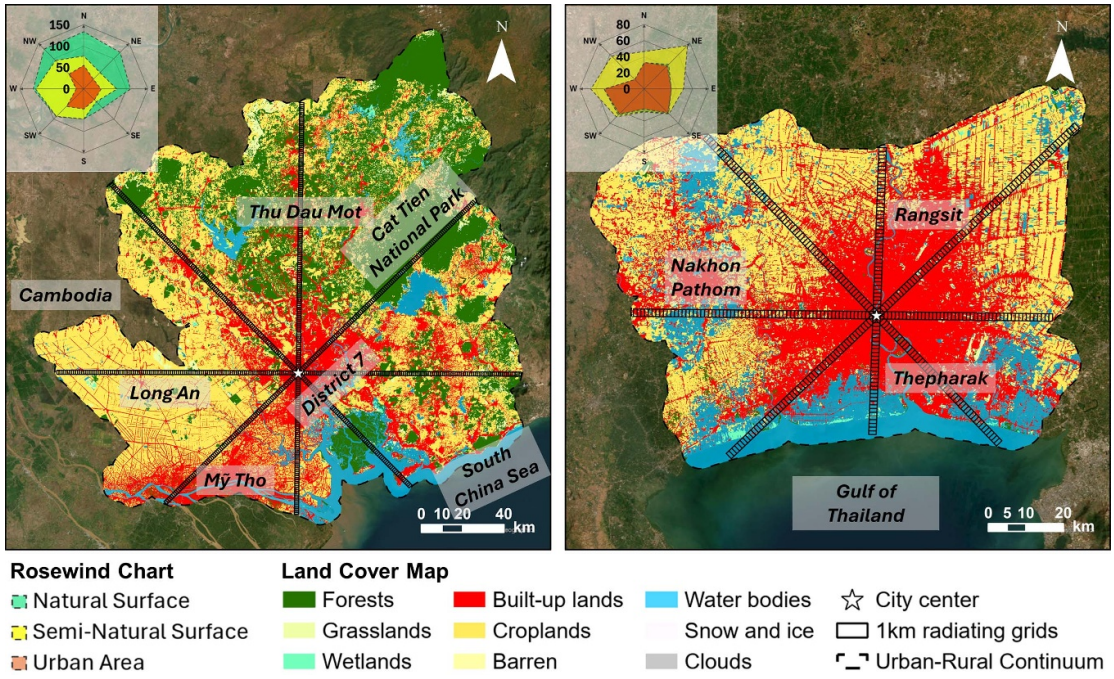


Figure 6. Land cover along the URCs from eight directions in Ho Chi Minh City (left) and Bangkok (right). The land use/land cover map of 2023 derived from Sentinel-2 (10 m resolution) by ESRI is used for illustration purposes. Detected as secondary urban centers, Thu Dau Mot (Ho Chi Minh City) and Rangsit and Thepharak (Bangkok), are highlighted on the maps. The relevant Windrose charts on landscape composition are positioned in the upper-left corner of each map.

gradually decreases outward. In contrast, large multicentric cities often exhibit asymmetric structures shaped by irregular natural features, administrative boundaries, and planning policies (Cao *et al* 2019, Fan *et al* 2019, Chen *et al* 2021). Consequently, landscape asymmetry in large metropolitan regions should often be viewed objectively as an adaptive morphological response to complex factors, rather than as a negative deviation from the idealized symmetric structure.

The proposed analytical framework provides planners with a spatially explicit and effective approach for monitoring urban structure and identifying emerging secondary centers. Beyond methodological merits, this study also offers several implications for urban planning and policy in rapidly developing SEA cities. First, urban fringes typically exhibit a more heterogeneous and balanced mix of landscape classes compared to urban centers and rural areas, which are often dominated by a certain category. This dominance can signal reduced resilience and adaptability due to limited land-use diversity. The degree of heterogeneity in urban fringes should be carefully considered and leveraged to accommodate expansion while protecting ecological functions. Second, the logarithmic relationship between population density and directional asymmetry (appendix D) suggests that cities with lower population densities are particularly sensitive to small demographic increase. For these cities, early planning interventions, such as infrastructure investment and reserve area establishment, can substantially influence the future spatial configuration of the URC. Third, the consistent influence of natural features indicates that asymmetric growth is often structurally inevitable. Urban planning frameworks should therefore optimize existing asymmetric corridors. Development zones, transportation networks, and green space conservation strategies should be designed to align with these inherent geographic constraints. As SEA cities continue to evolve toward polycentric and highly asymmetric forms, such directional metrics can support scenario modeling, infrastructure prioritization, and targeted urban management. Incorporating these insights into long-term metropolitan planning could help ensure more resilient, compatible, and equitable urban development across the multiple URCs.

Though recent studies increasingly incorporate multi-source geospatial data to examine LULC patterns at local or regional scales, most research remains case specific. This study uses directional gradient analysis to comprehensively characterize landscape structures. This approach provides a quantitative link between classical urban models and the complex realities of contemporary cities (Vizzari and Sigura 2015, Ortiz-Báez *et al* 2021). Methodologically, this approach offers a substantial advancement in efficiency. In this research, the directional gradient grids encompass only 13.13% of the total URCs' area, while accurately characterizing the landscape structures in complex multicentric cities. A full-coverage benchmark analysis confirms the representativeness of this sampling scheme, demonstrating a strong linear correlation ($R^2 = 0.92$) with the total urban density

(appendix E). This effectiveness is attributable to the model's focus: grids cover 23.15% of urban areas compared to 12.21% and 9.48% coverage of semi-natural and natural surfaces, respectively. The gradient model naturally emphasizes the areas close to the city center, where landscape structures dominantly shape the overall URC.

Despite its overall effectiveness, the single-center directional gradient approach has inherent limitations when applied to highly complex, polycentric cities. The reliance on eight directional grids may overlook or underestimate significant secondary centers located between these axes. To address this limitation, future research could incorporate overlay analysis and partitioning adjustments for the concentric rings. Exceptional spatial characteristics may pose challenges for the effective application of the proposed analytical approach. For example, Naypyidaw, where urban density remains below 50% even in areas surrounding the city center, has the highest SHEI value among all the studied urban centers. Its URC displays unusual randomness and dispersion which are difficult to model accurately. Additionally, as an LULC-based study, the proposed analytical framework primarily captures horizontal landscape patterns and may not differentiate between high-rise districts and low-rise sprawl within urban areas. Urban asymmetry can also be affected by underground space utilization and 3D morphological variations. It is recommended that future studies integrate 3D datasets, such as LiDAR or high-resolution DEM, to address this issue.

5. Conclusion

This study develops and applies a directional gradient-based analytical framework to quantitatively characterize the asymmetric landscape structures of the URCs across 19 SEA cities. By integrating Windrose analysis, spatial statistics, and landscape indices, the proposed approach bridges classical urban theory with multisource geospatial data, offering a spatially explicit method that captures the asymmetric nature of the URCs. Methodologically, this approach demonstrates significant efficiency. By analyzing less than 15% of the total URCs' area, the framework effectively captures the critical asymmetric nature of the URCs. It offers a scalable and transferable tool for comparative urban studies in regions with complex natural conditions and intensified anthropogenic activities. Two specific conclusions can be drawn from this study on the URCs' asymmetric landscape:

First, landscape asymmetry is a fundamental and quantifiable property of SEA URCs. Urban fringes consistently exhibit the highest landscape heterogeneity, reflecting dynamic transitions between urban and non-urban land uses and indicating zones of elevated ecological and planning sensitivity. In contrast, urban centers are often dominated by a single category, signaling reduced resilience and adaptability.

Second, physical geography and anthropogenic factors jointly shape the orientation and magnitude of asymmetry. Natural features and administrative boundaries generate persistent directional constraints that influence URCs' urban structure. These conditions lead to characteristic asymmetric patterns in coastal cities, demonstrating how SEA cities diverge from the classic theoretical urban models. Intensified anthropogenic activities also exert a strong nonlinear influence on URCs' asymmetry. The identified logarithmic relationship reveals that population density has a positive influence on the degree of directional urban asymmetry, but this influence saturates in URCs with high population density.

Overall, the proposed analytical framework provides practical tools and reliable data to quantify the asymmetry of diverse URCs. These fundamental insights into urban structure have direct implications for sustainable planning and development. The findings also underscore the importance of adaptive planning for waterfront development, flood risk management, and guiding future expansion where feasible.

While this study focused primarily on land cover and urban density, future research could incorporate a broader range of socioeconomic and environmental variables. The application of very high-resolution imagery would further help tease apart the specific causes of the asymmetric nature observed in URCs across different global regions. By systematically comparing the similarities and differences between SEA and other regions, more unified and flexible URC models could be developed to better capture the complexity and diversity of global urban environments.

Acknowledgment

This work was supported by the Land Cover Land Use Change Program (LCLUC) of the National Aeronautics and Space Administration (NASA) (Grant number: 8NSSC24K0920).

Data availability statement

The data that support the findings of this study are openly available at the following URL/DOI: https://livingatlas.arcgis.com/landcoverexplorer/#mapCenter=31.20320%2C29.94069%2C11.00&mode=step&timeExtent=2017%2C2024&year=2024 (Karra *et al* 2026).

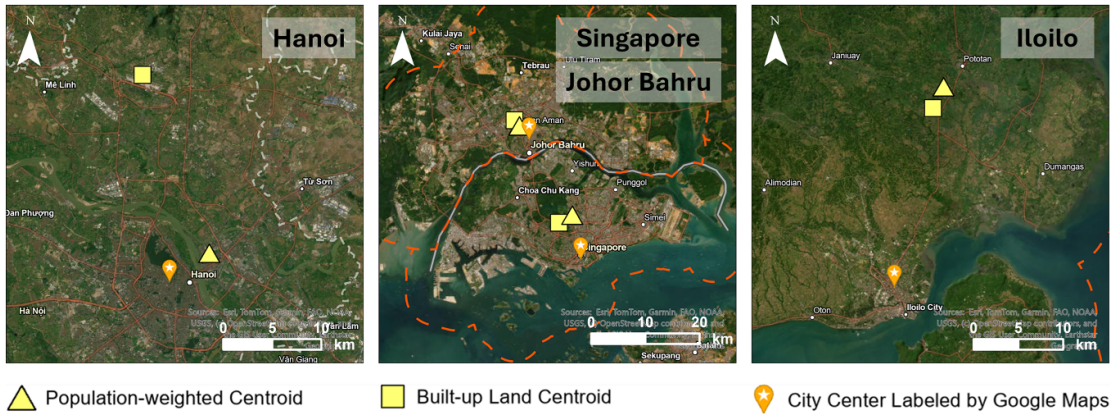


Figure A1. Comparison of approaches for determining the city center. The maps illustrate the locations of the population-weighted centroid, built-up land centroid, and the city name label from Google Maps across URCs of Hanoi, Singapore, Johor Bahru, and Iloilo. Influenced by asymmetrical urban morphologies and coastal constraints, the mathematical centroids demonstrate spatial deviations from the traditional CBDs.

Appendix A. Comparative validation of city center determination approaches

The centers of the 19 selected Urban Regional Cores (URCs) in this study were defined using geocoded coordinates from Google Maps (table 2). These labels represent consensus-based functional city centers, typically anchored to well-known civic or administrative landmarks such as city halls, major squares, or historically recognized cores. To evaluate the robustness of the city center definition adopted in this study, we conducted a comparative validation across all the studied URCs using two alternative mathematical centroid approaches: (1) population-weighted centroid and (2) built-up land centroid (figure A1). In addition, nightlight-based centroids were found to be geographically proximate to the built-up land centroids.

Across the 19 URCs examined, deviations are observed between mathematical centroids and the traditional CBDs. For population-weighted centroids, the minimum, median, and maximum distances from the traditional CBD are 2.73 km (Bangkok), 8.04 km (Denpasar), and 24.5 km (Pakse), respectively. For built-up land centroids, the corresponding distances are 4.56 km (Bandung), 10.28 km (Yangon), and 26.14 km (HCMC). Figure A1 presents representative examples illustrating these deviations. In Hanoi, the population-weighted centroid is located 5.15 km from the traditional CBD and falls within Long Bien district on the east bank of the Red River. Long Bien was incorporated as an urban district only in 2003 and does not represent the traditional or administrative core of Hanoi, which is historically situated on the west bank. In Singapore, the built-up land centroid deviates by 7.99 km from the traditional center and is positioned within the Singapore Island Country Club, a recreational green space that does not function as a central urban node. Even in cases with mathematical centroids relatively close to the traditional center, functional city centers are not captured because of the influence of urban morphology and spatial configuration.

In some relatively compact and morphologically regular URCs, such as Johor Bahru, mathematical centroids appear spatially closer to the traditional center. However, most mathematical centroids exhibit a high degree of randomness across the diverse geographies of SEA. In contrast, Google Maps city labels are typically anchored to historically recognized civic or administrative centers and benefit from continuous crowdsourced correction, providing a more stable and functionally grounded reference point. For the purposes of gradient-based directional landscape analysis, this functional center definition ensures greater methodological consistency and cross-city comparability.

Appendix B. Asymmetry quantification along the Urban–Rural Gradient

Directional differences in urban density peak at the urban fringe. Directional asymmetry is quantified using the standard deviation of urban density across the eight directions at 1 km intervals from the city center. To quantify a city density's asymmetric structure, STD_s was applied, and the eight radial directions at a given distance were used as the sample of the corresponding circular ring (figure B1). In almost all cases, STDs are low near the urban center and low again in the far rural area. It reaches its peak in the urban–rural fringe where the contrast among different types of landcover is the highest. This implies that the greatest directional differences of urban density occur at the transition between the city's center and rural sides: in some sectors the urban influence extends far outward, while in others it tapers

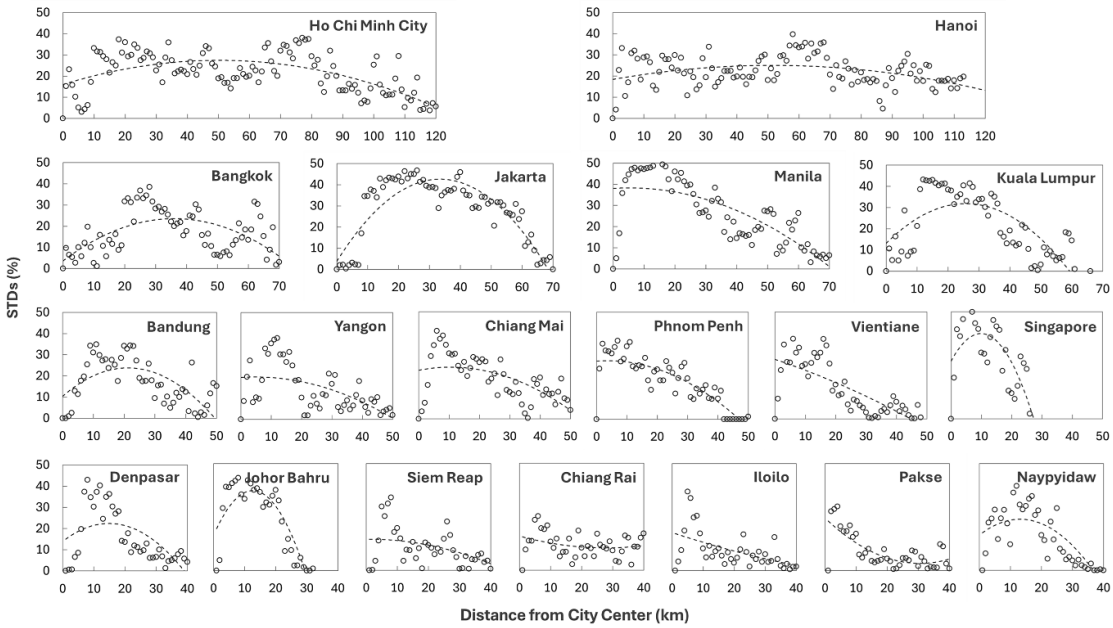


Figure B1. Changes in sample standard deviation (STD_s) of urban density with distance from the city center to rural landscapes across 19 study cities in Southeast Asia. STD_s at each distance is calculated based on urban density values from eight directions (figure 1). The smooth lines represent quadratic fits based on the least squares method.

off quickly. To quantitatively model this trend, we applied a quadratic model fitted via least squares. This model was selected because it theoretically captures the expected unimodal form of land heterogeneity while offering superior statistical performance (mean $R^2 = 0.47$ across all 19 URCs) compared to other conventional fitting functions, such as linear or logarithmic alternatives. For most studied cities, changes in STDs with distance are well-approximated by this function, where the vertex of the quadratic curve marks the estimated position of the urban fringe. However, it is worth noting that the quadratic function does not fit well with a few cases such as Chiang Rai and Siem Reap. This is because although the peak at the urban fringe is still present as a general pattern among these URCs, the decline in STDs beyond the fringe is much slower than the increase from the center to the fringe. This skewed pattern makes it difficult for a strictly axisymmetric quadratic function to capture the unimodal curves.

Appendix C. Quadratic fitting asymmetry–distance relationships across representative cities

Figure C1 illustrates this relationship for four representative cities of varying sizes, from the large city of Ho Chi Minh City to the more compact Johor Bahru. In this model, **y** represents the STD_s of the urban density across eight directions, and **x** is the distance from the city center. The vertex, the highest point of the curve, of the quadratic fit marks the characteristic radius of the urban–rural fringe. The quadratic curvature, controlled by the second-order coefficient a, indicates how rapidly the STD_s changes. A steeper curvature (a larger negative value for a, e.g. Johor Bahru: $a = -0.13$) implies a narrow fringe where urban density drops off quickly. Conversely, a shallower curvature (a smaller negative value for a, e.g. Ho Chi Minh City: $a = -0.01$) suggests a more gradual transition, often seen in the largest cities.

The quadratic model fits well for most medium and large cities, revealing distinct regularities among URCs of different scales. First, the distance between the city center and the peak of asymmetry increases with city size, indicating that larger cities possess more extended fringe zones. Second, the curvature flattens as city size increases, demonstrating that transitions become more gradual in major metropolitan regions. Generally, this asymmetry-distance model suggests that as cities expand, the quadratic curve flattens, pushing the fringe outward and reducing the sharpness of the urban–rural boundary. Conversely, some smaller cities do not exhibit a clear peak suitable for quadratic fitting, reflecting a simpler and less varied urban structure across the entire URC.

Appendix D. Relationship between population density and landscape asymmetry

The results of this study indicate that directional asymmetry is strongly influenced by anthropogenic factors, including population density. By analyzing the relationship between population density and the directional asymmetry of urban density (STD_p in

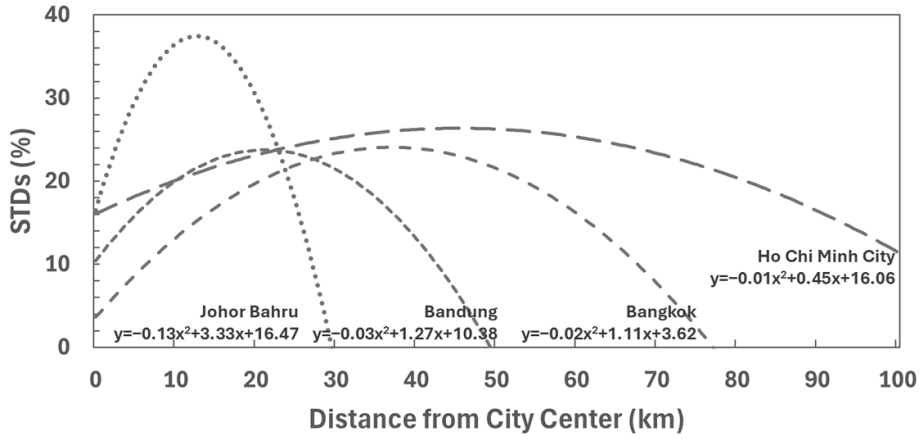


Figure C1. Quadratic model of urban density asymmetry for representative cities, Johor Bahru, Malaysia (small city), Bandung, Indonesia (medium city), Bangkok, Thailand (large city), and Ho Chi Minh City, Vietnam (large city). STD_s at each distance is calculated based on urban density values from eight directions.

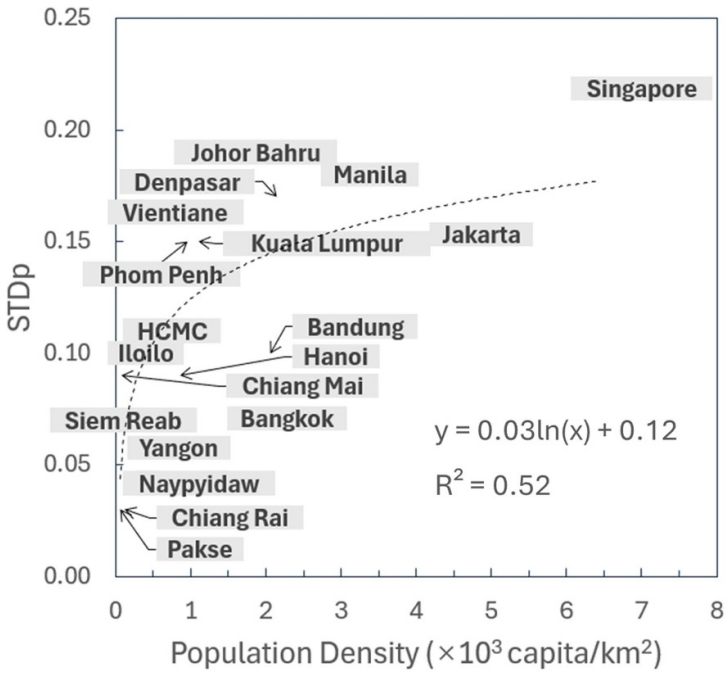


Figure D1. Scatter plot illustrating the relationship between directional asymmetry estimated by STD_p (table 5) and population density for the 19 studied URCs. The logarithmic correlation indicates that URCs with higher population densities tend to exhibit greater directional asymmetry in their urban spatial structure.

table 5), we identified a distinct logarithmic correlation: $y = 0.03ln(x) + 0.12$, with a high R^2 of 0.52 (figure D1). Notably, this logarithmic correlation has a distinct tipping point at around 1600 capita/km^2, indicating that for cities with lower population densities (e.g. Chiang Rai and Pakse), landscape asymmetry is extremely sensitive to population changes. In this phase, small increases in density drive rapid differentiation in urban structure, likely as early development expands along specific corridors (e.g. roads or rivers) while leaving other sectors undeveloped. Conversely, for metropolises with high population density (e.g. Jakarta, Manila, Singapore), the sensitivity of asymmetry to population growth diminishes significantly. While these cities exhibit the highest absolute asymmetry values, the rate of increase slows, suggesting that once a city establishes a mature, highly asymmetric structure, further densification tends to consolidate existing patterns rather than create a remarkably higher level of directional asymmetry.

Appendix E. Validation of sampling efficiency for the directional gradient model

To validate the representativeness and efficiency of the directional gradient sampling scheme, a full-coverage

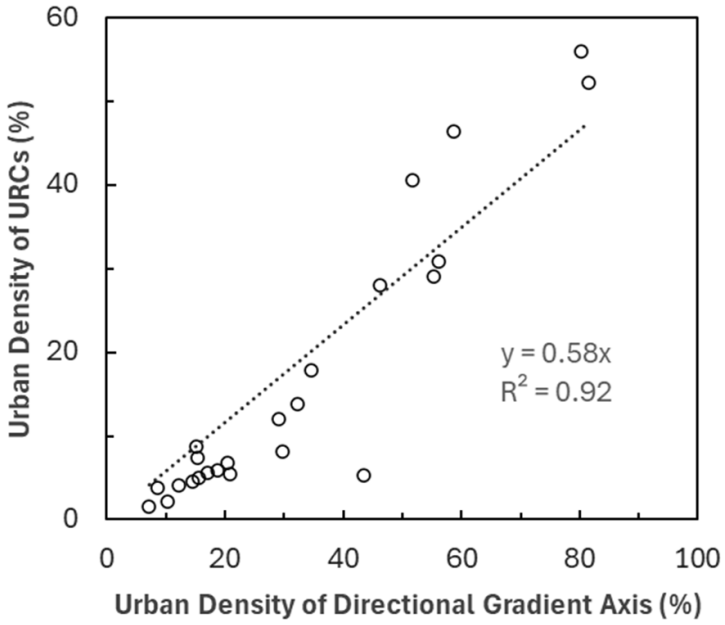


Figure E1. Linear regression and scatter plot comparing the urban density derived from the full-coverage URC area (D_u) and the directional gradient grids (D_g). The 24 data points represent the eight directional sectors of Jakarta, Chiang Mai, and Iloilo.

benchmark analysis was conducted. We randomly selected three URCs representing different size categories: Jakarta (Large), Chiang Mai (Medium), and Iloilo (Small). To ensure methodological consistency, the entire area of each URC was partitioned into eight directional sectors (North, Northeast, East, Southeast, South, Southwest, West, and Northwest) to align with the directional structure of the gradient grids. For each of the 24 sectors (3 cities × 8 directions), we calculated the urban density using both the full-coverage URC area (D_u) and the directional gradient grids (D_g).

As shown in figure E1, the correlation analysis reveals a strong linear relationship between the gradient grid-captured urban density and the full-coverage urban density, with an R^2 of 0.92. As expected, D_g values are systematically higher than D_u because the directional grids consistently include the urban center, where built-up intensity is highest. However, the stable linear relationship demonstrates that the proposed sampling framework properly reflects the directional asymmetry of the whole URC.

ORCID iDs

Jin Wang 0000-0003-2584-9644
Jiquan Chen 0000-0003-0761-9458
Peilei Fan 0000-0003-4448-4281
Jiaguo Qi 0000-0002-8183-0297
Atul K Jain 0000-0002-4051-3228
Karen Seto 0000-0002-4928-2446

References

Barnes W, Pagano L, Pagano T S and Salomonson V V 2002 Prelaunch characteristics of the moderate resolution imaging spectroradiometer (MODIS) on EOS-AM1 *IEEE Trans. Geosci. Remote Sens.* **36** 1088–100

Bell M M 1992 The Fruit of difference: the rural-urban continuum as a system of identity *Rural Soc.* **57** 65–82

Boongla Y, Chanonmuang P, Hata M, Furuuchi M and Phairuang W 2021 The characteristics of carbonaceous particles down to the nanoparticle range in Rangsit city in the Bangkok Metropolitan Region, Thailand *Environ. Pollut.* **272** 115940

Burgess E W 1925 The growth of the city: an introduction *Urban Ecology* (Springer) pp 71–78

Cao H, Liu J, Chen J, Gao J, Wang G and Zhang W 2019 Spatiotemporal patterns of urban land use change in typical cities in the Greater Mekong Subregion (GMS) *Remote Sens.* **11** 801

Cao Y, Fang C, Li G, Feng Y, Li L and Sun J 2026 Asymmetric thermal effects of urban vegetation greening and browning *Land Use Policy* **160** 107833

Cattaneo A, Adukia A, Brown D L, Christiaensen L, Evans D K, Haakenstad A, McMenomy T, Partridge M, Vaz S and Weiss D J 2022 Economic and social development along the urban–rural continuum: new opportunities to inform policy *World Dev.* **157** 105941

Chen J *et al* 2018 Prospects for the sustainability of social-ecological systems (SES) on the Mongolian plateau: five critical issues *Environ. Res. Lett.* **13** 123004

Chen J, Park H, Fan P, Tian L, Ouyang Z and Lafortezza R 2021 Cultural landmarks and urban landscapes in three contrasting societies *Sustainability* **13** 4295

Cumming G S, Barnes G and Southworth J 2008 *Environmental Asymmetries Complexity Theory for a Sustainable Future* (Columbia University Press)

Dai E, Wang Y, Ma L, Yin L and Wu Z 2018 "Urban-rural" gradient analysis of landscape changes around cities in mountainous regions: a case study of the Hengduan Mountain region in Southwest China *Sustainability* **10** 1019

Downes N K, Storch H, Viet P Q, Diem N K and Dinh L C 2024

Assessing peri-urbanisation and urban transitions between 2010 and 2020 in Ho Chi Minh city using an urban structure type approach *Urban Sci.* **8** 11
ESRI 2024 Sentinel-2 10m land use/land cover time series (available at: www.arcgis.com/home/item.html?id=cfcb7609de5f478eb7666240902d4d3d)
Fan P *et al* 2022 Urbanization, economic development, and environmental changes in transitional economies in the global south: a case of Yangon *Ecol. Process.* **11** 65
Fan P, Ouyang Z, Nguyen D D, Nguyen T T H, Park H and Chen J 2019 Urbanization, economic development, environmental and social changes in transitional economies: Vietnam after Doimoi *Lands. Urban Plann.* **187** 145–55
Fujii T and Hartshorni T A 1995 The changing metropolitan structure of Atlanta, Georgia: locations of functions and regional structure in a multinucleated urban area *Urban Geogr.* **16** 680–707
Gluch R M and Ridd M K 2010 The V-I-S model: quantifying the urban environment *Remote Sensing of Urban and Suburban Areas* (Springer) pp 85–116
Harris C D and Ullman E L 1945 The nature of cities *ANNALS Am. Acad. Political Soc. Sci.* **242** 7–17
Hedlund M 2016 Mapping the socioeconomic landscape of rural Sweden: towards a typology of rural areas *Reg. Stud.* **50** 460–74
Hoyt H 1939 *The Structure and Growth of Residential Neighborhoods in American Cities* (US Government Printing Office)
HSBC 2024 The next level: how Southeast Asia is moving up the value chain (available at: www.business.hsbc.com/en-gb/insights/growing-my-business/the-next-level-how-southeast-asia-is-moving-up-the-value-chain)
IMF 2024 World Economic Outlook (October 2024): real GDP growth (available at: www.imf.org/external/datamapper/NGDP_RPCH@WEO/OEMDC/ADVEC/WEOWORLD)
Jiao L 2015 Urban land density function: a new method to characterize urban *Lands. Urban Plann.* **139** 26–39
Karlsson S 1986 The applicability of wind profile formulas to an urban-rural interface site *Bound. Layer Meteorol.* **34** 333–55
Karra K, Kontgis C, Statman-Weil Z, Mazzariello J C, Mathis M and Brumby S P 2026 *Sentinel-2 10m Land Use/Land Cover Time Series* (available at: https://livingatlas.arcgis.com/landcoverexplorer/)
Kodl G, Streeter R, Cutler N and Bolch T 2024 Arctic tundra shrubification can obscure increasing levels of soil erosion in NDVI assessments of land cover derived from satellite imagery *Remote Sens. Environ.* **301** 113935
Lebakula V *et al* 2024 *LandScan Silver Edition* (Oak Ridge National Laboratory)
Li X, Yu L and Chen X 2023 New insights into urbanization based on global mapping and analysis of human settlements in the Rural–Urban Continuum *Land* **12** 1607
Loveland T R and Belward A S 1997 The international geosphere biosphere programme data and information system global land cover data set (DIScover) *Acta Astronaut.* **41** 681–9
Lu D and Weng Q 2006 Use of impervious surface in urban land-use classification *Remote Sens. Environ.* **102** 146–60
Nguyen H, Behre E, Nguyen H K L, Pham G T, Vu B T, Egerer M and Bachofer F 2025 Forest dynamics mapping in central Vietnam from 1988 to 2022 using Landsat time-series data *Environ. Res. Lett.* **20** 074048
ORNL, & NASA 2019 Shannon Diversity: richness and Evenness (available at: https://modis.ornl.gov/documentation/shannon.html)
Ortiz-Báez P, Cabrera-Barona P and Bogaert J 2021 Characterizing landscape patterns in urban-rural interfaces *J. Urban Manage.* **10** 46–56
Pahl R E 1966 The rural-urban continuum *Sociol. Ruralis* **6** 299–329
Peng J, Hu Y, Liu Y, Ma J and Zhao S 2018 A new approach for urban-rural fringe identification: integrating impervious surface area and spatial continuous wavelet transform *Lands. Urban Plann.* **175** 72–79
Phiri D, Simwanda M, Salekin S, Nyirenda V R, Murayama Y and Ranagalage M 2020 Sentinel-2 data for land cover/use mapping: a review *Remote Sens.* **12** 2291
Prime Minister of Vietnam 2025 Decision No. 202/QD-TTg on approving the general planning project of Ho Chi Minh City and Thu Duc City to 2040 (available at: https://qhkt.hochiminhcity.gov.vn/Uploads/Document/Legislation/202_QD-TTg_21012025_2-signed.pdf)
Qi Y, Henderson M, Xu M, Chen J, Shi P, He C and Skinner G W 2004 Evolving core-periphery interactions in a rapidly expanding urban landscape: the case of Beijing *Landscape Ecol.* **19** 375–88
Sarker T, Fan P, Messina J P, Macatangay R, Varnakovida P and Chen J 2024b Land surface temperature and transboundary air pollution: a case of Bangkok Metropolitan Region *Sci. Rep.* **14** 10955
Sarker T, Fan P, Messina J P, Mujahid N, Aldrian E and Chen J 2024a Impact of urban built-up volume on urban environment: a case of Jakarta *Sustain. Cities Soc.* **105** 105346
Schneider A *et al* 2015 A new urban landscape in East-Southeast Asia 2000–2010 *Environ. Res. Lett.* **10** 034002
Schwirian K 2007 Ecological models of urban form: concentric zone model, the sector model, and the multiple nuclei model *The Blackwell Encyclopedia of Sociology* (Wiley)
Shannon C E 1948 A mathematical theory of communication *Bell Syst. Tech. J.* **27** 379–423
Skinner G W 2002 Marketing and social structure in rural China *Etudes Rurales* **2** 161–2
Stokes E C and Seto K C 2019 Characterizing and measuring urban landscapes for sustainability *Environ. Res. Lett.* **14** 045002
Tian L and Chen J 2022 Urban expansion inferenced by ecosystem production on the Qinghai-Tibet plateau *Environ. Res. Lett.* **17** 035001
UN Population Division 2024 World population prospects (available at: https://population.un.org/wpp/)
Van de Voorde T, Jacquet W and Canters F 2011 Mapping form and function in urban areas: an approach based on urban metrics and continuous impervious surface data *Lands. Urban Plann.* **102** 143–55
Vichiensan V, Wasuntarasook V, Hayashi Y, Kii M and Prakayaphun T 2022 Urban rail transit in Bangkok: chronological development review and impact on residential property value *Sustainability* **14** 284
Vizzari M, Hilal M, Sigura M, Antognelli S and Joly D 2018 Urban-rural-natural gradient analysis with CORINE data: an application to the metropolitan France *Lands. Urban Plann.* **171** 18–29
Vizzari M and Sigura M 2015 Landscape sequences along the urban-rural-natural gradient: a novel geospatial approach for identification and analysis *Lands. Urban Plann.* **140** 42–55
Wang J, Zhou W, Wang J and Yu W 2020 Spatial distribution of urban greenspace in response to urban development from a multi-scale perspective *Environ. Res. Lett.* **15** 064031
Weng Q and Lu D 2009 Landscape as a continuum: an examination of the urban landscape structures and dynamics of Indianapolis City, 1991–2000, by using satellite images *Int. J. Remote Sens.* **30** 2547–77
Wilkosz-Mamcarczyk M, Olczak B and Prus B 2020 Urban features in rural landscape: a case study of the municipality of Skawina *Sustainability* **12** 4638
Xu G, Jiao L, Liu J, Shi Z, Zeng C and Liu Y 2019 Understanding urban expansion combining macro patterns and micro dynamics in three Southeast Asian megacities *Sci. Total Environ.* **660** 375–83
Zhao J, Yu L, Zhao L, Fu H and Gong P 2025 Asymmetric influence of urban morphology changes on land surface

temperature between daytime and nighttime *Sustain. Cities Soc.* **124** 106307
Zheng M, Huang W, Xu G, Li X and Jiao L 2023 Spatial gradients of urban land density and nighttime light intensity in 30 global megacities *Hum. Soc. Sci. Commun.* **10** 404
Zheng Y, Tan J, Huang Y and Wang Z 2022 The governance path of urban–rural integration in changing urban–rural relationships in the metropolitan area: a case study of Wuhan, China *Land* **11** 1334
Zhu Y, Myint S W, Chen J, Fan P, Seto K C, Jain A, Qi J and Wang J 2025 Thermal changes along the urban–rural continuums in Southeast Asia *Environ. Res. Lett.* **20** 054051
Zorrilla-Miras P, Palomo I, Gómez-Baggethun E, Martín-López B, Lomas P L and Montes C 2014 Effects of land-use change on wetland ecosystem services: a case study in the Doñana marshes (SW Spain) *Lands. Urban Plann.* **122** 160–74